Role of Co^{2+} Incorporation in Significant Photocurrent Enhancement of Electrochemical Deposited CdSe Quantum Dots Sensitized TiO$_2$ Nanorod Arrays Solar Cells

Baoyuan Wang, Jun Zhang,Yunxia Hu, Shuqiang Wang, Rong Liu, Chao He, Xina Wang, Hao Wang[*]

Hubei Collaborative Innovation Center for Advanced Organic Chemical Materials, Faculty of Physics and Electronic Technology, Hubei University, Wuhan 430062, PR China
[*]E-mail: nanoguy@126.com

Cobalt doped CdSe quantum dots have been successfully synthesized on TiO$_2$ nanorod arrays using the electrochemical deposition method, and the effect of Co^{2+} content on the properties of CdSe/TiO$_2$ electrodes has been studied. It has been found that the introduction of Co^{2+} results in a decrease of deposited rate of CdSe and smaller crystallite size as the SEM figures shown. X-ray diffraction results reveal both undoped and Co-doped CdSe exhibit zinc blende structure without any impurity phase. In comparison with the pure CdSe/TiO$_2$ photoelectrode, the Co-doped CdSe/TiO$_2$ electrodes show the wider absorption range in visible region and the better band alignment for electron transport, which gives rise to the higher photocurrent density. Moreover, by adjusting the deposited electrical quantity and the amount of Co, the 2% in atomic ratio Co-doped CdSe/TiO$_2$ electrode with deposited electrical quantities at 0.9 C yields a largest saturated current density of 13.4 mA/cm^2 under the irradiation of AM1.5G simulated sunlight at 100 mW/cm^2. And the quantum dot sensitized solar cells using the TiO$_2$/Co-doped CdSe nanocable array as photoanode shows a power conversion efficiency of 1.225% which is higher than that of the pure CdSe photoanode (0.620%).

1. INTRODUCTION

Quantum dot sensitized solar cells (QDSSCs) are viewed as the most promising solar cells. This is mainly because they have the following advantages: the tunability of the band gap through changing the synthesis methods; high absorption coefficient; generation of multiple electron carriers under high energy excitation [1-8]. For these reasons, the QDSSCs are expected to boost the power

conversion efficiency of solar cells. Although the semiconductor nanocrystals have many potential advantages, the performance of QDSSCs is still much worse than that of dye sensitized solar cells (DSSCs) up to now, which may be due to the low open circuit potential as well as low fill factor. In order to improve the efficiency of the cells, many avenues have been tried, including use more than one sensitizer [9-13], optimization of QDs sensitized electrode structure [14-17], pretreating the photoanode with $TiCl_4$ [18], passivating the QDs with ZnS layer [19, 20], and introducing impurity to change intrinsic property of semiconductor nanocrystal [21,22]. Recently, researchers have found that the electrical and optical performance of quantum dots can be modified by doping of strong activity of transition metal elements. Therefore, study of the properties of QDs doped with transition metals such as manganese, iron, and cobalt is interesting. For example, Arora et al. found that the absorption edge of CdS nanoparticles showed red-shift in visible range after doping Fe^{2+} or Mn^{2+} [23,24]. Kamat et al. had succeeded in doping CdS semiconductor films with Mn^{2+} for designing high efficiency solar cells, which shown a high conversion efficiency of 5.4% using TiO_2/Mn-doped-CdS/CdSe as photoelectrode. This is the first report about QDSSCs with the high power conversion efficiency greater than 5%, and the high efficiency mainly results from the dopant in quantum dots, which can create electronic states in the midgap region of the QDs, thus altering the charge separation and recombination dynamics[25]. Zielinsk et al. reported that sp-d exchange interactions in Co^{2+}-doped II-VI semiconductor are much larger than those in Mn^{2+}-doped counterparts [26-28], so we predict that doping Co^{2+} has a greater effect on cells than doping Mn^{2+}.

In this work, CdSe quantum dots were deposited on single crystalline TiO_2 nanorod arrays which provide a direct pathway for electrons with few grain boundaries, and the Co^{2+} were deliberately added into the electrolyte during electrodeposition of CdSe quantum dots. The effect of Co^{2+} dopant on the properties of CdSe /TiO_2 electrodes has been studied. In comparison to the CdSe/TiO_2 system, the Co-doped CdSe/TiO_2 photoelectrode exhibit better photoelectrochemical activity due to the enhancement of photo absorption and the band alignment.

2. EXPERIMENTAL SECTION

All the chemicals were of analytic grade and used without further purification. Titanium butoxide, concentrated hydrochloric acid (HCl, 36.5%-38% by weight) and deionized water were used as titanium precursor, acidic medium and solvent, respectively. In a typical synthesis, 8ml of deionized water, 0.2 ml of titanium butoxide and 8 ml hydrochloric acid were mixed in a Teflon-lined autoclave of 20-ml capacity under magnetic stirring. A piece of FTO substrate, through an ultrasonically cleaning with acetone, anhydrous alcohol, and deionized water, was placed within the reactor. Subsequently, the autoclave was sealed and maintained at 150 ℃ for 10 h, followed by natural cooling to room temperature. After synthesis, the FTO substrate, on which TiO_2 nanorod arrays had been grown, was taken out, rinsed extensively with deionized water, and dried in ambient air. The TiO_2 nanorod arrays were annealed at 500℃ for 2 h in the air atmosphere.

The electrochemical deposition of the CdSe quantum dots was then carried out in an electrochemical workstation (CH instrument, model 660B) with a three-electrode system. The TiO_2

nanorod arrays-on-FTO, a standard saturated calomel electrode (SCE), and Pt foil were used as the working electrode, the reference electrode, and the counter-electrode, respectively. The electrolyte was made up of an aqueous solution of 0.05 M Anhydrous sodium sulfite ($NaSO_3$), 0.025 M Selenium (Se), 0.05M nitrilotriacetic acid trisodium salt (NTA, $C_6H_6NO_6Na_3$), and 0.025 M cadmium acetate ($CdC_4H_6O_4$). In order to incorporate the Co^{2+}, a required amount of cobalt acetate was deliberately added into the electrolyte. The electrodeposition was performed at a fixed potential of -1.0 V versus SCE. Both deposition time and the total charge passing through the electrodes were varied, which determined the deposited quantity of QDs.

The morphology of photoelectrode was observed using a JEOL F6700 field emission scanning electron microscope (FESEM). The X-ray diffraction (XRD) for the crystal structure of the products was carried out in a Bruker D8 X-ray diffractometer. Uv-vis absorption spectra were recorded on UV-3000 spectrophotometer. The photoelectrochemical (PEC) cell was fabricated using a standard three-electrode configuration, with $FTO/TiO_2/CdSe$ and $FTO/TiO_2/Co$-doped CdSe as active photoelectrode, Pt sheet as a counter electrode and Ag/AgCl electrode as a reference electrode. A mixture of 0.5M S and 0.3 M Na_2S aqueous solution was used as electrolyte and sacrificial reagent to maintain the stability of CdSe. An AM1.5G light with a power of 100 mW/cm^2 was used as the illumination source. The QDSSCs were prepared with a TiO_2/Co-doped CdSe photoelectrode and a Pt/FTO counter electrode, and the polyiodide electrolyte was used as redox couple. Photocurrent density-voltage (J-V) curves were recorded using a keithley 2400 digital multimeter.

3. RESULTS AND DISCUSSION
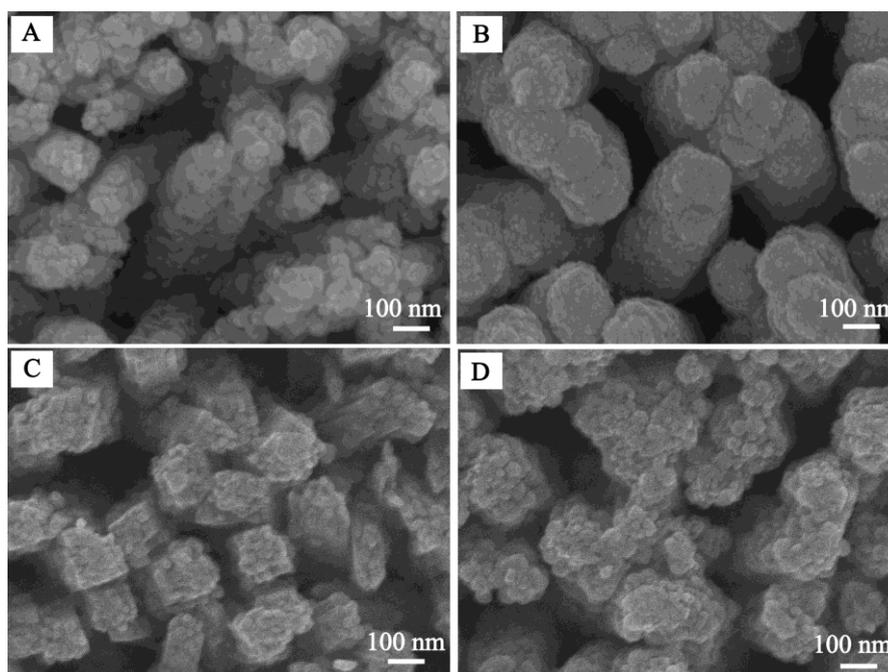
Figure 1. Typical FESEM images of undoped CdSe and Co-doped CdSe sensitized TiO_2 nanorod arrays at different deposited electrical quantities. (A) CdSe (0.3C) (B) CdSe (0.6C) (C) Co-doped CdSe (0.3C) (D) Co-doped CdSe (0.6C).

The surface morphology of CdSe and Co-doped CdSe sensitized TiO_2 nanorod arrays was studied using FESEM. As shown in figure 1, the entire surface of the TiO_2 nanorods is covered by CdSe nanoparticles to form a TiO_2/CdSe nanocable structure, and the surface of nanocable had became rough after CdSe deposited. In addition, we can note that the Co^{2+} incorporation affected the morphology of photoelectrodes. Comparing the top view of the FTO/TiO_2/CdSe (figure A, B) photoelectrode with the FTO/TiO_2/ Co-doped CdSe photoelectrode (figure C, D), it can be found that TiO_2 nanorod arrays sensitized by Co-doped CdSe shows smaller diameter than the undoped CdSe nanocable and the deposition rate becomes slow as the Co^{2+} adding to electrolyte when the deposition electrical quantity is identical.
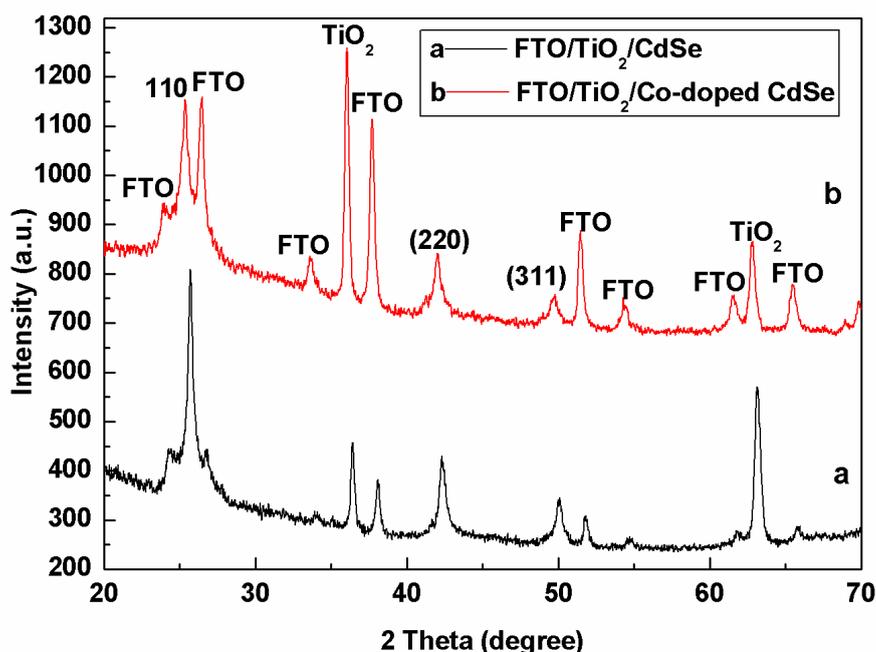
Figure 2. XRD pattern of CdSe (a) and Co-doped CdSe (b) sensitized TiO_2 nanorod arrays.

Figure 2 shows the XRD of CdSe and Co-doped CdSe sensitized TiO_2 nanorod arrays. Peaks assigned to the FTO substrate are detected, which has a rutile SnO_2 structure (JCPDS no.46-1088). The diffraction peaks index as TiO_2 reveal that the TiO_2 nanorods have a tetragonal rutile structure (JCPDS No. 89-4920), which can be attributed to the small lattice mismatch between FTO and rutile [29], and the enhanced (002) peak located at 62.89° indicates that the nanorods are well crystallized and grow in [001] direction with the growth axis parallel to the substrate surface normal. In addition to the diffraction peaks of SnO_2 and TiO_2, the diffraction peaks at 2θ valuing 25.62°, 42.12°and 49.72°are indexed as (111), (220), and (311) planes, corresponding to cubic zinc blende structure of CdSe (JCPDS no.88-2346). As shown in figure 2, the peaks in the diffraction pattern of Co-doped CdSe (curve b) also match well with the standard diffraction pattern of CdSe crystal; there are no detectable phases of Co clusters or cobalt oxide within the sensitivity limitation of XRD. Moreover, we can calculate the average crystallite size using Scherrer's formula [30]

$$D = \frac{K\lambda}{\beta \cos\theta} \quad (1)$$

Where D is the grain size, K is a constant taken to be 0.94, λ is the wavelength of x-ray radiation, βis the the full widths at half-maximum (FWHMs), and θis the angle of diffraction. The particle size of CdSe and Co-doped CdSe nanoparticle was evaluated to be 13 nm and 10 nm, so the Co doped sample have a smaller crystallite size than the undoped CdSe, which is well consistent with the results of SEM.
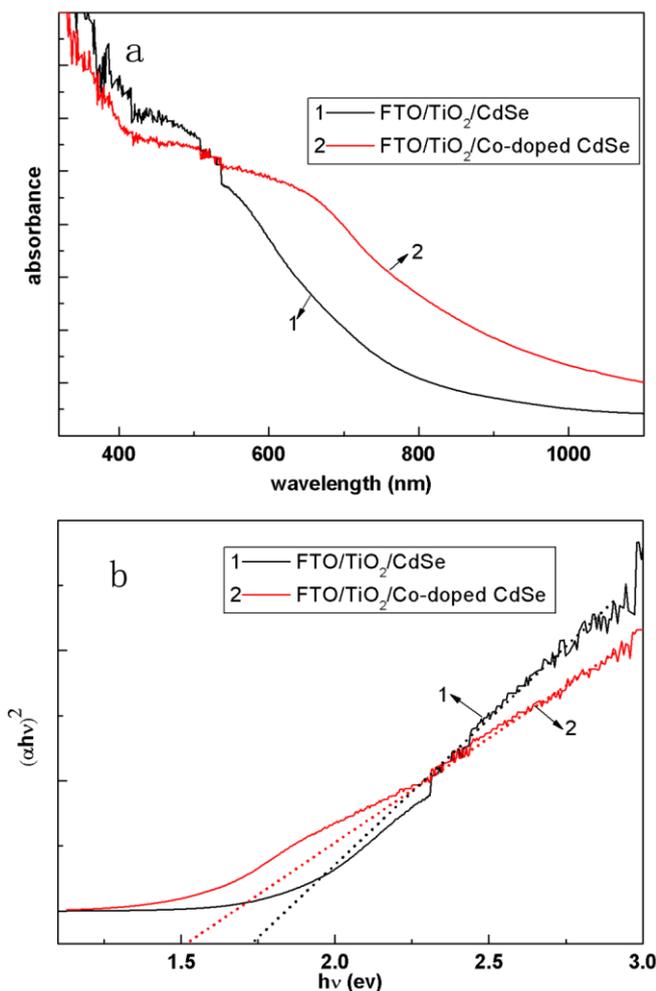
Figure 3. (a)Uv-vis absorption spectra of undoped CdSe and Co-doped CdSe sensitized TiO_2 nanorod arrays. (b) $(\alpha h\nu)^2$ versus hν plot for determining band gap of QDs in undoped and Co-doped samples

The optical performance of CdSe and Co-doped CdSe coated TiO_2 nanorod arrays are characterized by absorbance. The figure 3a shows the Uv-vis absorption spectra of the two samples. The absorption in the visible region is remarkably enhanced in comparison with bare TiO_2, indicating the efficient photosensitization of CdSe QDs, and the Co-doped sample show higher absorption in visible region than the undoped CdSe. The exact band gap values can be obtained by employing a

Tauc analysis of $(h\nu\alpha)^2$ versus hv plots derived from the absorption spectra (figure 3a) [31]. As shown in figure 3b, extrapolation of the linear part until its intersection with the hv-axis give the value of band gap, which is determined as 1.73 ev for undoped sample and 1.52 ev for Co-doped sample. So we can conclude that the incorporation of cobalt ion narrowed the band gap of CdSe, and extended the absorption wavelength range. According to the literature [32-35], the presence of transition metal ions in semiconductor introduces new energy levels into the band gap of semiconductor. Therefore, the absorption enhancement and narrow band gap in Co^{2+} doped CdSe come from the electronic transition from the dopant energy level (Co^{2+}) to the conduction band of CdSe.
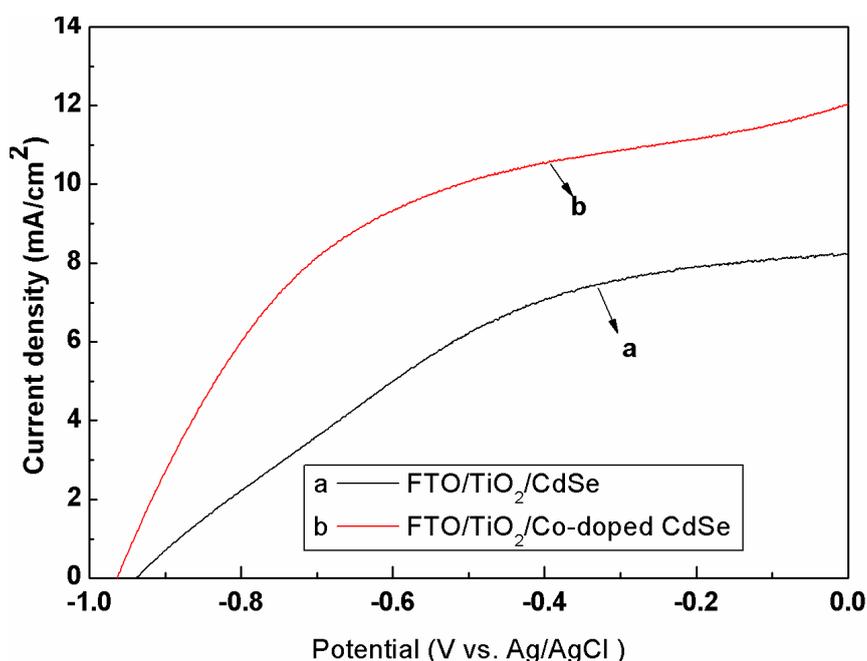
Figure 4. Current density versus potential curves for FTO/TiO₂/CdSe and FTO/TiO₂/Co-doped CdSe photoelectrodes measured under illumination of AM 1.5 light at 100 mW/cm².

Using the FTO/TiO₂/CdSe and FTO/TiO₂/Co-doped CdSe nanocable arrays as the photoelectrodes, a three-electrode PEC configuration is carried out to obtain their photovoltaic performance. Figure 4 shows the current density versus potential characteristics of the above PEC cells under the illumination of AM 1.5 light at 100 mW/cm². The saturated current density of FTO/TiO₂/CdSe nanocable arrays is ~ 8.23 mA/cm², and the FTO/TiO₂/Co-doped CdSe nanocable photoelectrode shows a better photocurrent density of ~ 11.97 mA/cm², which is 43.9% higher than that of undoped photoelectrode. This result can be understood as follows: the incorporation of cobalt results in the narrower band gap, so the Co-doped CdSe photoelectrode exhibits better optical absorption in visible region as the photo absorption curve shown (figure 3), and the more photon will be absorbed by CdSe QDs which give rise to the higher photocurrent density.

Another reason for the difference of photoelectrochemical performance can be attributed to the band alignment. Here, the dark J-V curves of FTO/TiO₂/CdSe and FTO/TiO₂/Co-doped CdSe

nanocable arrays are given in figure 5. The Co-doped photoelectrode presents higher current density as the same bias potential is applied, suggesting that the photoelectrode has a lower resistance and a superior band edge structure more favorable for charge transfer than the FTO/TiO$_2$/CdSe photoelectrode. The shift of the Fermi level of CdSe can be qualitatively evaluated by the open circuit potentials (OCP) from figure 5. When the semiconductor contact with an electrolyte containing a redox couple, the Fermi level of the semiconductor and electrolyte will be identical once reaching the electrostatic equilibrium, and the equilibrium Fermi level of the electrode is equivalent to the OCP measured in dark conditions [36, 37].
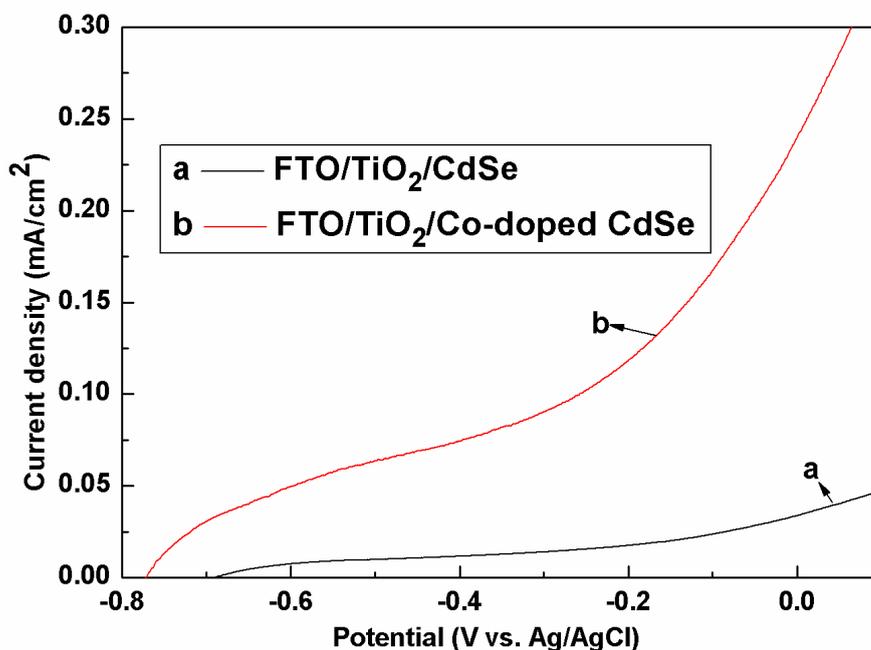
Figure 5. Current density versus potential curves for FTO/TiO$_2$/CdSe and FTO/TiO$_2$/Co-doped CdSe photoelectrodes measured in dark conditions.
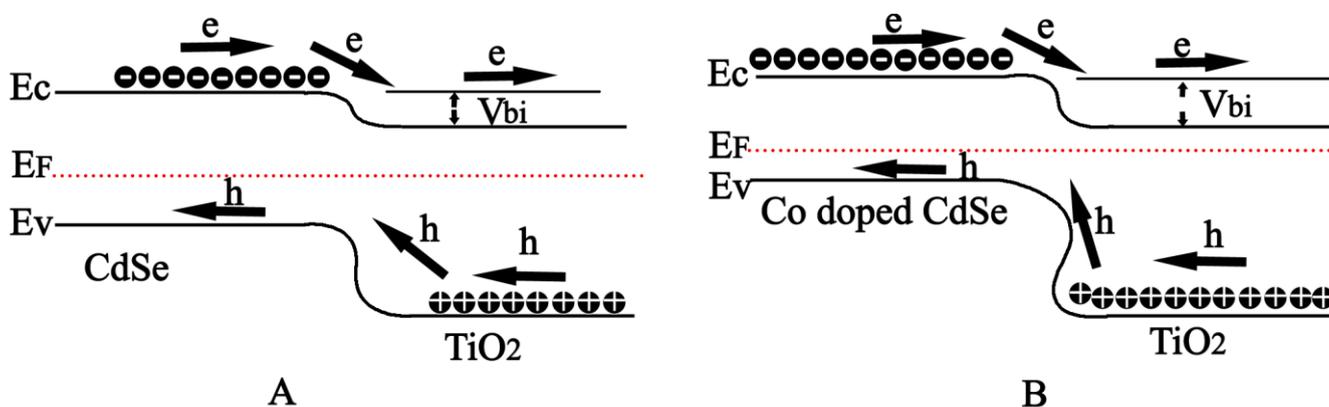
Figure 6. Relative Fermi level and band edge position of FTO/TiO$_2$/ CdSe (A) and FTO/TiO$_2$/Co-doped CdSe (B)

As the figure 5 shows the OCP measured for the FTO/TiO$_2$/Co-doped CdSe (-0.77 V) photoelectrode is higher than that of FTO/TiO$_2$/ CdSe (-0.69 V), implying that Co doped CdSe has a higher Fermi level in comparison with undoped CdSe. The relative Fermi level and the band edges position of FTO/TiO$_2$/CdSe and FTO/TiO$_2$/Co-doped CdSe photoelectrode are schematically illustrated in figure 6. After the contacting of TiO$_2$ and CdSe, their Fermi level will be flattened, and the TiO$_2$ and CdSe have the same Fermi level as the figure 6 shown. The Co-doped CdSe (Figure 6A) shows a higher Fermi level of -0.77 V in comparison with undoped CdSe (Figure 6B), which cause the upward shift both of the conduction band minimum and valence band maximum of CdSe, indicating the band offset between Co-doped CdSe and TiO$_2$ is higher than that of undoped CdSe. The built–in potential (V$_{bi}$) of FTO/TiO$_2$/Co-doped CdSe photoelectrode, originated from the conduction band offset between QDs and TiO$_2$, is higher than that of FTO/TiO$_2$/CdSe photoelectrode. This favors for charge transfer and gives rise to bigger photocurrent.
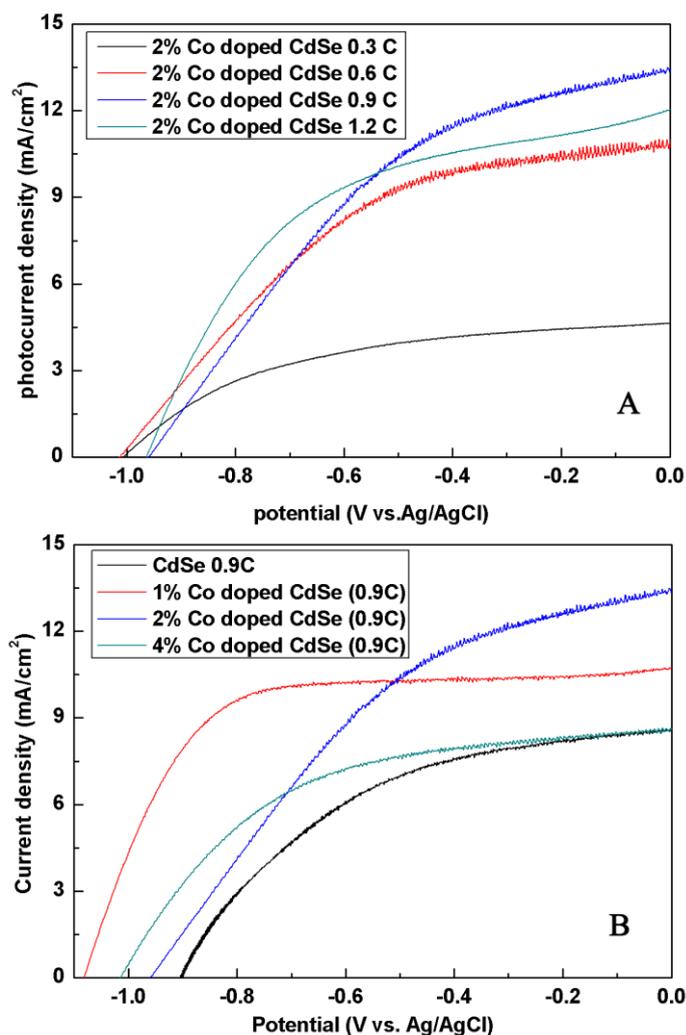
Figure 7. Current density versus potential curves for FTO/TiO$_2$/Co-doped CdSe photoelectrodes with various deposition electrical quantities (A) and different amount of impurity (B) measured under illumination of AM 1.5G light at 100 mW/cm^2

Figure 7A shows the current density versus potential characteristics of PEC cell with various deposition electrical quantities, and the amount of Co dopant was maintained at 2% in atomic ratio. It is observed from figure 7A that the saturated current density increases initially with the increasing of deposition quantity until it reaches a maximum value, then decreases with the deposition quantity. A largest photocurrent density of 13.42 mA/cm^2 is observed with zero bias potential (vs.Ag/AgCl electrode) when the deposited electrical quantity is 0.9 coulomb. Compared with recently reported photocurrent densities for photoelectrodes that are similar, usually less than 10 mA/cm^2 [38-40], our results suggest that Co doped CdSe photoelectrodes have superior photoelectrochemical properties.

It is noteworthy that the amount of CdSe QDs deposited on the TiO$_2$ nanorods increases with the deposited electrical quantity, which helps to enhance the visible light absorption. Therefore, at the beginning, the photocurrent intensity enhances as the electrical quantity increases. But when the amount of CdSe QDs goes on increasing, the CdSe layer will become thicker to block the gap of the TiO$_2$ nanorods, which leads to the nanorods touch each other and form a film structure. Such a structure is very adverse for the electrolyte to penetrate in. Thus, the photogenerated holes in CdSe can not be effectively separated via the electrolyte, leading to insufficient charge transfer and transport. Figure 7B gives the current density versus potential curves for FTO/TiO$_2$/Co-doped CdSe photoelectrodes with different amount of impurity as the electrical quantity were kept at 0.9C. It apparently indicates from the figure 7B that the saturated current density increases with the increase of cobalt concentration up to 2 at.%, while for further increase in cobalt concentration the photocurrent density value is found to decrease. The photoelectrode with 2 at.% cobalt doped shows a maximum photocurrent density of 13.42 mA/cm^2, which is about 63% larger than that of undoped samples. When the cobalt concentration is 4 at.%, the photoelectrode has the same photocurrent density as the undoped sample, so in order to improve the photocurrent density, the cobalt concentration have an optimum value.
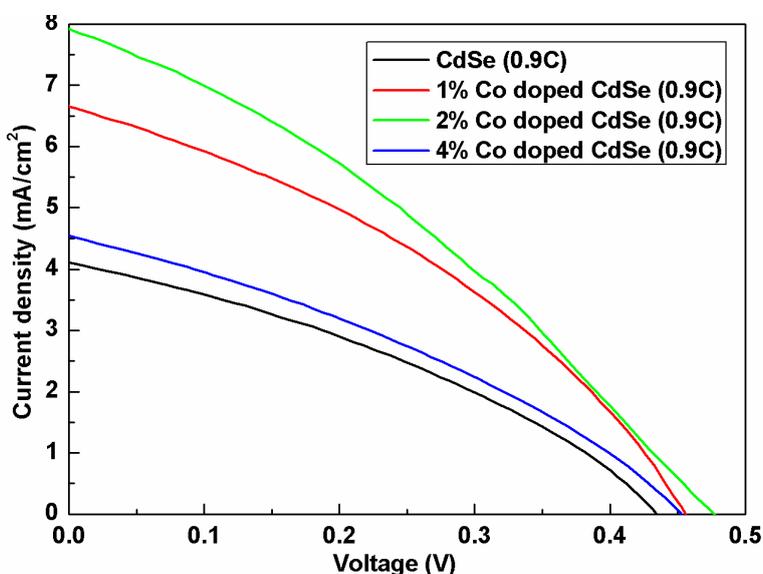
Figure 8. the J-V curves of the QDSSCs based on TiO$_2$/Co-doepd CdSe nanocable arrays with different amount of Co under illumination of AM 1.5 light.

The TiO$_2$/Co-doped CdSe nanocable arrays with different amount of Co dopant were sandwiched and bonded with Pt counter electrodes to construct quantum dots sensitized solar cells. The internal space of the cells was filled with a polyiodide electrolyte which was used as redox couple. The active area of the solar cells was 0.14 cm^2, the photovoltaic characteristic of the solar cells was measured using a solar simulator with 100 mW/cm^2 irradiation (AM 1.5). Figure 8 shows the J-V curves of QDSSCs using the TiO$_2$/Co-doped CdSe as photoelectrode, and the photovoltaic characteristics of these devices with different amount of Co dopant are summarized in Table1. Series resistance Rs and shunt resistance Rsh were evaluated from the slopes of J-V curves using the relation [41]

$$\left(\frac{dI}{dV}\right)_{I=0} \cong \left(\frac{1}{Rs}\right) \quad (2)$$

$$\left(\frac{dI}{dV}\right)_{V=0} \cong \left(\frac{1}{Rsh}\right) \quad (3)$$

In table 1, the TiO$_2$/CdSe device shows an open circuit voltage (Voc) of 0.435V, a short circuit density (Jsc) of 4.11 mA/cm^2, fill factor (FF) of 0.347 and power conversion efficiency (η) of 0.620%. When the 1 at. % Co dopant was incorporated; slightly changes in Voc and FF values were obtained. Remarkably, the Jsc increases from 4.11 to 6.66 mA/cm^2, which result in a enhancement of η from 0.620% to 1.103%. And when the cobalt concentration reach up to 2 at.%, a highest η of 1.225% was obtained, due to a drastically increase in the Jsc from 4.11 to 7.91 mA/cm^2 compared to undoped CdSe. While for further increase in cobalt concentration, the Jsc, Voc, and η were found decrease. As the table1 shown, the introduction of Co^{2+} gave rise to the higher PCE, which may be due to the better optical absorption and higher V$_{bi}$ than that of pure CdSe photoanode. Similar results have been reported by Yadav for Fe doped CdSe thin films by spray pyrolysis technique [42]. In his study, the best obtained for conversion efficiency is 1.48% at 0.30 mol% Fe, which is three times more than the one for pure CdSe (0.50%) material

Table 1. photovoltaic properties parameters of QDSSCs based on TiO2/Co-doped CdSe nanocable arrays with different amount of impurity.

sample	Jsc (mA/cm^2)	Voc (V)	FF	h (%)	Rs (Ω)	Rsh (KΩ)
CdSe	4.11	0.435	0.347	0.620	338	1.47
1% Co doped CdSe (0.9C)	6.66	0.455	0.364	1.103	286	1.11
2% Co doped CdSe (0.9C)	7.91	0.476	0.325	1.225	183	0.72
4% Co doped CdSe (0.9C)	4.54	0.452	0.336	0.690	246	1.16

In addition, in table1, it can be seen that Rsh and Rs changes with the amount of Co incorporation in CdSe QDs. Both the Rsh and Rs decrease with increase in Co incorporation concentration attain minimum values at 2 at. % and then increase with further increase in Co incorporation concentration. The Rs change is favor for power conversion efficiency, but the Rsh change is detrimental. The contributions to Rs come from the change of charge carrier concentration as the Co^{2+} introducing, and the variation of Rsh may be due to the interface change between CdSe QDs and TiO_2 nanorods when the Co dopant is incorporated.

4. CONCLUSION

CdSe and Co-doped CdSe quantum dots were deposited on TiO_2 nanorod arrays using electrochemical deposition method. The effect of cobalt impurity on the performance of $CdSe/TiO_2$ photoelectrodes has been studied. The result shows that the incorporation of Co^{2+} from the deposition electrolytes into CdSe quantum dots gives rise to higher photocurrent density than the undoped CdSe. Based on UV-vis absorption analysis, the higher current density results from the narrower band gap as the cobalt introduction. Another reason for the higher current density attributed to the band alignment, the incorporation of cobalt results in bigger V_{bi}, which lead to bigger photocurrent. By adjusting the deposited electrical quantity and the amount of Co impurity, Co-doped $CdSe/TiO_2$ electrode yielded a largest saturated current density of 13.4 mA/cm^2 under the irradiation of AM1.5G simulated sunlight at 100 mW/cm^2. And the quantum dot sensitized solar cells (QDSSCs) using the TiO_2/Co-doped CdSe nanocable array as photoanode show a higher power conversion efficiency of 1.225% than that of the pure CdSe photoanode of 0.620%.

References

1. A.J.Nozik, *Physica E,* 14 (2002) 115.
2. R. D. Schaller and V.I. Klimov, *Phys.rev.Lett.* 92 (2004) 186601.
3. K. K. Anusorn, T. Kevin, T. Kensuke, K. Massaru, V. K. Prashant, *J. AM. Chem.Soc.* 130 (2008) 4007.
4. J. H. Ahn, R. S. Mane, V. V. Todkar and S. H. Han, *Int. J. Electrochem. Sci.*2 (2007) 517.
5. N. A. Hamizi, M. R. Johan, *Int. J. Electrochem. Sci.* 7 (2012) 8473.
6. X. N. Wang, H. J. Zhu, Y. M. Xu, H. Wang, Y. Tao, S. K. Hark, X. D. Xiao, and Q. Li, *ACS Nano.* 4 (2010) 3302.
7. J. F. Galloway, J. Park, K. H. Lee, D. Wirtz, P. C. Searson, *Sci. Adv. Mater.* 1 (2009) 93.
8. S. Rawalekar, M. V. N. Raj, H. N. Ghosh, *Sci. Adv. Mater.* 4 (2012)637.
9. G. M. Wang, X. Y. Yang, F. Qian, J. Z. Zhang, Y. Li, *Nano Lett.* 10 (2010) 1088.
10. Y. L. Lee, C. F. Chi, and S. Y. Liau, *Chem. Mater.* 22 (2010) 922.
11. Y. H. Zhang, J. Zhu, X. C. Yu, J. F. Wei, L. H. Hu, S. Y. Dai, *Solar Energy.* 86 (2012) 964.

12. Z. Z. Lu, J. Xu, X. Xie, H. K. Wang, C. D. Wang, S. Y. Kwok, T. L. Wong, H. L. Kwong, I. Bello, C. S. Lee, S. T. Lee, and W. J. Zhang, *J. Phys. Chem. C.* 116 (2012) 2656.
13. J. P. Deng, M. Q. Wang, X. H. Song, Y. H. Shi, X. Y. Zhang, *J. Colloid Interface Sci.* 388 (2012) 118.
14. H. Wang, Y. Bai, H. Zhang, Z.H. Zhang, J. H. Li, L. Guo, *J. Phys. Chem.C.* 114 (2010) 16451.
15. J. Zhou, B.Song, G. L. Zhao, W. X. Dong, G. R. Han, *Appl Phys A* 107 (2012) 321.
16. W. T. Sun, Y. Yu, H. Y. Pan, X. F. Gao, Q. Chen, and L. M. Peng, *J. AM. Chem.Soc.*130 (2008) 1124.
17. T. Ling, M. K. Wu, K. Y. Niu, J. Yang, Z. M. Gao, J. Sun, and X. W. Du, *J. Mater. Chem.* 21 (2011) 2883.
18. F. Y. Zhao, G. S. Tang, J. B. Zhang, Y. Lin, *Electrochimica Acta* 62 (2012) 396.
19. S. Hachiya, Q. Shen, and T. Toyoda, *J. Appl. Phys.* 111 (2012) 104315.
20. S. W. Jung, J. H. Kim, H .Kim, C. J. Choi, K. S. Ahn, *Current Applied physics* 12 (2012) 1459.
21. N. Pradhan, D. D. Sarma, *J. Phys. Chem. Lett.* 2 (2011) 2818.
22. X. Y. Yu, B. X. Lei, D. B. Kuang, and C. Y. Su, *Chem.Sci.* 2 (2011) 1396.
23. S. Arora and S. Sundar Manoharan, *Solid State Commun.*144 (2007)319.
24. N. Badera, B. Godbole, S.B. Srivastava, P.N. Vishwakarma, L.S. Sharath Chandra, D. Jain, M. Gangrade, T. Shripathi, V.G. Sathe, and V. Ganesan, *Appl. Surf. Sci.* 254 (2008) 7042
25. K. S. Pralay, V. K. Prashant. *J. AM. Chem.Soc.* 134 (2012)2508.
26. M. Zielinski, C. Rigaux, A. Lemaitrie, and A. Mycielskin, *Phys. Rev. B* 53 (1996)674.
27. M. J. Seong, H. Alawadhi, I. Miotkowski, and A.K. Ramdas, *Phys. Rev. B* 63 (2001) 125208.
28. M. Thambidurai, N. Muthukumarasamy, D. Velauthapillai, S. Agilan, and R. Balasundaraprabhu, *J. Electron. Mater.* 41 (2012) 4.
29. B. Liu, and E. S. Aydil, *J. AM. Chem.Soc.* 131(2009)3985
30. N. Dixit, H. Soni, M. Chawda, and D. Bodas, *Mater.Lett.* 63 (2009) 2669.
31. S. Monticone, R. Tufeu, A. V. Kanaev, *J.Phys.Chem.B* 102 (1998) 2854.
32. K. Nagaveni, M.S. Hegde, G. Madras, *J. Phys. Chem. B* 108 (2004) 20204.
33. T. Umebayashi, T. Yamaki, H. Itoh, K. Asai, *J. Phys. Chem.* Sol. 63 (2002) 1909.
34. K. Elghniji, A. Atyaoui, S. Livraghi, L. Bousselmi, E. Giamello, M. Ksibi, *J. Alloys. Comp.* 541 (2012) 421-427.
35. J. Zhu, F. Chen, J. Zhang, H. Chen, M. Anpo, *J. Photochem. Photobiol. A* 180 (2006) 196.
36. V. Chikan, *J. Phys. Chem. Lett.* 2 (2011) 2783.
37. H. Wang, T. Wang, X. N. Wang, R. Liu, B.Y. Wang, H.B. Wang, Y. Xu, J. Zhang, J. X. Duan *J.Mater.Chem.*22 (2012)12532.
38. Y. W. Tang, X. Y. H, M. J. Chen, L. J. Luo, B. H. Li, L. Z. Zhang, *Electrochim. Acta* 54 (2009) 2742.
39. B. H. Bang, and P. V. Kamat, *Adv. Funct. Mater.* 20 (2010) 1970.
40. Y. T. Li, L. Wei, R. Z. Zhang, Y. X. Chen, and J. Jiao, *J. Nanomater* 1155 (2012) 103417.
41. T. J. Coutts, *Sol. Energy. Mater.* 50 (1978) 99.
42. A. A. Yadav, *J. Alloys. Comp.* 552 (2013) 318